Proceedings of Global Power and Propulsion Society
ISSN-Nr: 2504-4400
GPPS Hong Kong 2023
October 17-19, 2023
www.gpps.global

GPPS-TC-2023-0164

Acceleration of Large-Eddy Simulation Using Harmonic Balance Method for Unsteady Flows with Low Non-dimensional Frequency

Yuma Iwamoto
Department of Aeronautics and Astronautics, The University of Tokyo
iwamoto@thermo.t.u-tokyo.ac.jp
7-3-1 Hongo, Bunkyo-ku, Tokyo, Japan

Susumu Teramoto
Department of Aeronautics and Astronautics, The University of Tokyo
teramoto@thermo.t.u-tokyo.ac.jp
7-3-1 Hongo, Bunkyo-ku, Tokyo, Japan

Koji Okamoto
Department of Advanced Energy, The University of Tokyo
k-okamoto@edu.k.u-tokyo.ac.jp
5-1-5 Kashiwanoha, Kashiwa-shi, Chiba, Japan

ABSTRACT

Harmonic Balanced Large-Eddy Simulation(HB-LES) is proposed for the efficient high-fidelity simulation of the unsteady flows with low non-dimensional frequency. Harmonic balance method for unsteady RANS simulation is originally introduced to large-eddy simulation, utilizing the difference in timescales between the period flow and the turbulent fluctuations. Periodic flow and turbulent fluctuation are computed without disregarding their nonlinear mutual interference by iterating short-time large-eddy simulation and harmonic balance method. Evaluation computations of HB-LES are performed for Srokes Boundary Layer at Reynolds number of 1790 and pitching NACA0012 airfoil. The accuracy and computational efficiency of the HB-LES are discussed by comparing with the conventional large-eddy simulation and experimental results.

INTRODUCTION

An accurate prediction of cascade flutter is the key to the improved aerodynamic design of turbomachinery. As the separation, transition, compressibility, and their nonlinear interaction are important in cascade flutter(Mayle, 1991; Denton, 2010), scale-resolving simulation, where turbulent fluctuation are directly resolved, is desired for the reliable prediction. Large-eddy simulation(LES) is a promising scale-resolving simulation particularly in engineering (Slotnik et al., 2014; Gourdain et al., 2014).

Huge computational cost accompanied by the large number of time steps remains a major obstacle for the LES of cascade flutter. The number of time steps is almost inversely proportional to non-dimensional frequency in the conventional LES. As the non-dimensional frequency of cascade flutter in axial compressor is as low as 0.1, resulting total number of time steps can exceed 10^7. The numerical cost of such redundant time integrations is still prohibitively large for daily-use in industrial application, A substantial improvement in computational efficiency is required to perform the LES of cascade flutter in industrial design.

In order to establish a computationally efficient scale-resolving simulation for cascade flutter, authors are developing acceleration method for the LES of the oscillating flows with the low non-dimensional frequency. The key idea(Iwamoto et al., 2022) is to introduce the harmonic balance method(Hall et al., 2002), which is an efficient RANS simulation technique for periodic flows, into the LES. In this paper, we plesent the implementation of the idea, harmonic balanced large-eddy simulation(HB-LES), and the results of evaluation computations.

NUMERICAL METHOD

Governing Equations

The oscillating turbulent flow with the low non-dimensional frequency $S_t = (L/U)/T$ of approximately 0.1 or less, defined by representative length L, representative velocity U and period T, is discussed in this study. Given that L/U corresponds approximately to the timescale of the largest turbulent eddies, the period is orders of magnitude longer than the timescale of turbulent fluctuations. Fig.1 is a typical time history of a physical quantity in a oscillating turbulent flow with the low non-dimensional frequency. The physical quantity is composed of a periodic component with long timescale, represented by the orange dash line, and nonperiodic turbulent fluctuations with a short timescale, solid blue line.

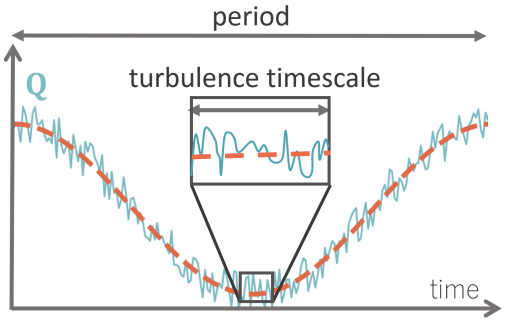

Figure 1 Oscillating Turblent Flow with Low Non-dimensional Frequency.

The Navier-Stokes equation for a three-dimensional compressible viscous flow is given by

$$\frac{\partial \mathbf{Q}}{\partial t} = \mathbf{R}(\mathbf{Q}) \tag{1}$$

where the conservative variables are $\mathbf{Q} = (\rho, \rho u, \rho v, \rho w, e)^T$. $\mathbf{R}(\mathbf{Q})$ on the right-hand side includes the convective fluxes, viscous terms, and source terms. Spatial parameter $\mathbf{x}$ and temporal parameter t of the conservation variables $\mathbf{Q}(\mathbf{x}, t)$ are omitted for clarity when not necessary.

Physical quantity $\mathbf{Q}$ is decomposed into periodic components $\hat{\mathbf{Q}}$ and nonperiodic turbulent fluctuations $\mathbf{Q}'$ as

$$\mathbf{Q} = \hat{\mathbf{Q}} + \mathbf{Q}' \tag{2}$$

Assume that a frequency f_c which satisfies $f_p \ll f_c \ll f_t$ exists, where f_p is the frequency of the highest harmonic component of $\hat{\mathbf{Q}}$ and f_t is the representative frequency of $\mathbf{Q}'$. Let L be a low-pass filter that passes only frequencies bellow f_c. The periodic component is extracted by applying L to the conservative variables. Similarly, the time derivatives of the periodic component is extracted.

$$L[\mathbf{Q}] = \hat{\mathbf{Q}}, \qquad L\left[\frac{\partial \mathbf{Q}}{\partial t}\right] = \frac{\partial \hat{\mathbf{Q}}}{\partial t} \tag{3}$$

Applying L to both sides of Eq.(1) gives the following equation:

$$\frac{\partial \hat{\mathbf{Q}}}{\partial t} = L[\mathbf{R}(\mathbf{Q})] \tag{4}$$

The governing equation for the periodic component $\hat{\mathbf{Q}}$ is formally derived by using $\mathbf{R}(L[\mathbf{Q}]) = \mathbf{R}(\hat{\mathbf{Q}})$ as

$$\frac{\partial \hat{\mathbf{Q}}}{\partial t} = \mathbf{R}(\hat{\mathbf{Q}}) + \mathbf{S} \tag{5}$$

$$\mathbf{S} = L[\mathbf{R}(\mathbf{Q})] - \mathbf{R}(L[\mathbf{Q}]) \tag{6}$$

The second-order moments between turbulent fluctuation $\mathbf{Q}'$ and periodic component $\hat{\mathbf{Q}}$ are in $\mathbf{S}$ in Eq.(5). Hereafter, $\mathbf{S}$ defined in Eq.(6) is referred to as the mutual interaction term.

For the turbulent fluctuations $\mathbf{Q}'$, substitution of Eq.(2) into Eq.(1) gives its governing equation, i.e.,

$$\frac{\partial \mathbf{Q}'}{\partial t} = \mathbf{R}(\hat{\mathbf{Q}} + \mathbf{Q}') - \frac{\partial \hat{\mathbf{Q}}}{\partial t} \tag{7}$$

Harmonic Balanced Large-Eddy Simulation; HB-LES

Fig.2 illustrates the proposed method harmonic balanced large-eddy simulation; HB-LES. The HB-LES alternatively iterates the LES- and HB-stage. The LES-stage is a set of large-eddy simulations based on Eq.(7) at each time-level. The simulation time of each LES is shorter than the period of the oscillation while sufficiently long compared to the turbulent timescale. The HB-stage is a convergence calculation of harmonic balance method(Hall et al., 2002, 2013) based on Eq.(5). Between two stages, the mutual interaction term $\mathbf{S}$ (Eq.(6)) is transferred from the LES-stage to HB-stage, and $\hat{\mathbf{Q}}$ and $\frac{\partial \hat{\mathbf{Q}}}{\partial t}$ are transferred from the HB-stage to LES-stage. The iteration is repeated until the HB-stage solution $\hat{\mathbf{Q}}$ does not change between stages.

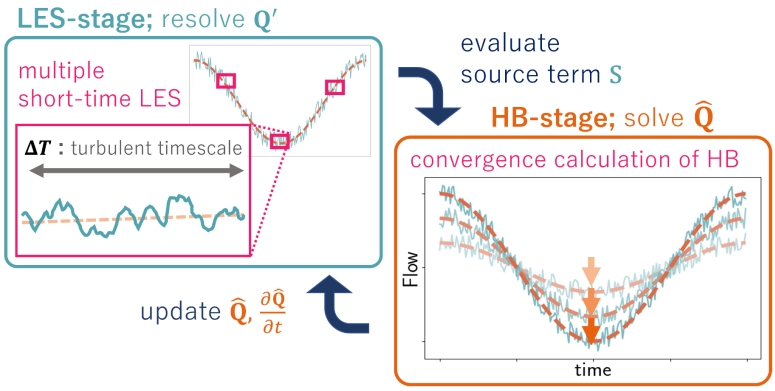

Figure 2 Schematic Diagram of the HB-LES.

Both periodic component $\hat{\mathbf{Q}}$ and turbulent component $\mathbf{Q}'$ obtained at the final stage of HB-LES are consistent with the result of conventional LES of the Navier-Stokes equation (1). This is because $\hat{\mathbf{Q}}$ is the solution of Eq.(5), $\mathbf{Q}'$ is the solution of Eq.(7), the information of the periodic component is properly transferred from the HB-stage to the LES-stage through $\hat{\mathbf{Q}}$ and $\frac{\partial \hat{\mathbf{Q}}}{\partial t}$, and the information of the turbulent fluctuation is properly transferred from the LES-stage to the HB-stage through $\mathbf{S}$. The last point is not self-evident; however, because the simulation time of the LES-stage is significantly shorter than the period of the oscillation while it is sufficiently long compared to the turbulent timescale, the time averaging over LES-stage works as the low-pass filter L that has the cut-off frequency f_c of $f_p < f_c < f_t$. Therefore, the mutual interaction term $\mathbf{S}$ defined by Eq.(6) is properly evaluated from the result of the LES-stage.

The simulation time of LES-stage is set to approximately $S_t T$ in this study. If homogeneous directions for periodic component $\hat{\mathbf{Q}}$ exist, spatial averaging in such directions could be employed as the low-pass filter in addition to the time averaging. Another example of averaging operation is the dual-mesh methods(Xiao and Jenny, 2012; He and Yi, 2019), in which turbulent fluctuations are resolved with a fine mesh in LES and their statistics are interpolated to a coarse mesh in HB using an appropriate spatial smoothing.

EVALUATION OF THE HB-LES

The HB-LES is implemented extending the in-house code which has been widely applied to compressible turbulence(Fujii and Obayashi, 1989; Kurokawa et al., 2020; Teramoto, 2005; Teramoto et al., 2017).

In the LES-stages, a 2nd-order backward ADI-SGS with 4 internal iterations is used for the time integration. The governing equation is three-dimensional compressible Navier-Stokes equation. Implicit LES with no SGS term is performed. The tri-diagonal sixth-order compact differencing scheme(Kim and Lee, 1996, 2011) is used for the advection and diffusion terms. The eighth-order compact filter(Gaitonde and Visbal, 2000) with the filter coefficient $\alpha = 0.495$ is applied to the conservative variables at each iteration in order to eliminate aliasing errors.

In the HB-stages, 1st-order Roe scheme is used for the advection term, 2nd-order central differencing scheme for the diffusion term, and pseudo-time marching with ADI-SGS for convergence calculation.

Stokes Boundary Layer

The free-stream oscillates with a zero-mean harmonic velocity $U(t) = U_0 sin(\omega t)$ in Stokes boundary layer problem. the Reynolds number $Re_{\delta_S} = U_0 \delta_S / \nu$ based on the amplitude of the freestream velocity U_0 and the Stokes-layer thickness $\delta_S = \sqrt{2\nu/\omega}$ is 1790. The flow oscillation is driven by the sinusoidally vibrating body force $U_0 \omega cos(\omega t)$. U_0 is coressponding to the Mach number $M_0 = 0.15$ and the non-dimensional frequency $\omega H / U_0$ based on channel height H is 0.034.

The computational domain is $50\delta_S \times 40\delta_S \times 25\delta_S$ for the sreamwise(x), normal(y), and spanwise(z) directions with $131 \times 255 \times 131$ grid points. The maximum grid spacing are $\Delta x^+ = 24, \Delta y^+{}_{min} = 0.3, \Delta z^+ = 12$. The flow is periodic for the streamwise and spanwise directions. The computational domain is half of the channel, and the top surface is the channel

center. Slip and no-slip wall boundary conditions were imposed at top and bottom boundary, respectively.

The simulation time of each LES-stage $\Delta T = 1/100T$ is chosen based on the convergence of the two-time correlation of velocity fluctuations. $1/100T$ corresponds to 1.5 Flow-Through-Time and $75\delta_S/U_0$, which is sufficiently long for the convergence of the turbulent statistics. In the HB-stages, the number of harmonics $N = 10$ is chosen based on a preliminary consideration with reference to previous studies(Salon et al., 2007; Jensen et al., 1989).

Fig.3 shows the normalized streamwise mean velocity profiles for every 30°. The results of the proposed method are compared with the experiment(Jensen et al., 1989) and the conventional LES(Salon et al., 2007). The results of HB-LES are quantitatively in good agreements with both of the experiment and conventional LES for most of the phases.

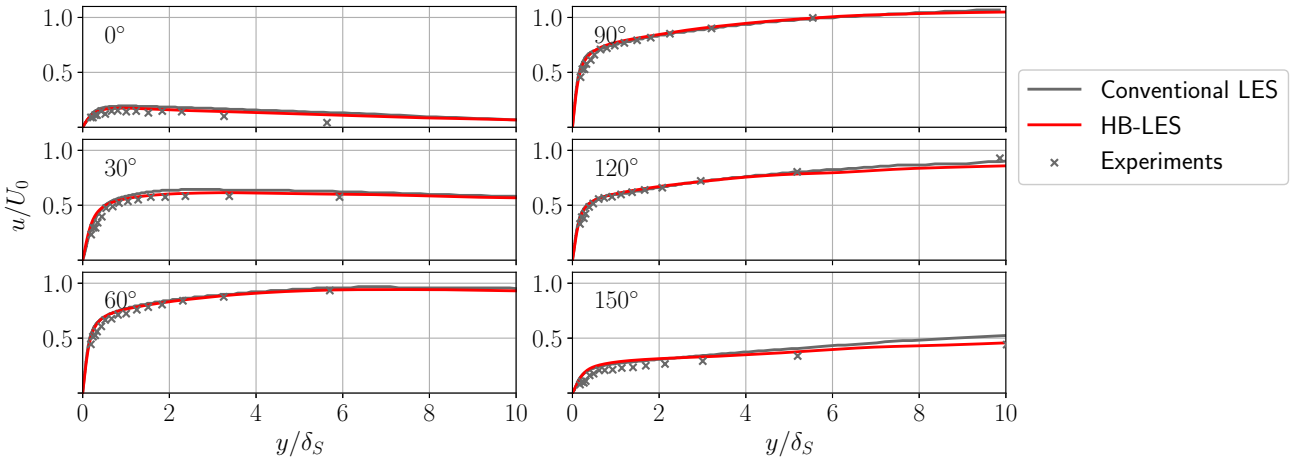

Figure 3 Non-dimensional Mean Velocity Profiles, red line: proposed method, black line: conventional LES(Salon et al., 2007), black cross: experimental data(Jensen et al., 1989).

Fig.4 shows the normalized wall-shear stress over 1 period. The HB-LES shows good agreement with the experimental results(Jensen et al., 1989), generally within the range of scatter of the experimental results. HB-LES is also in good agreement with the conventional LES(Salon et al., 2007) except for a difference of 10% in the peak values. HB-LES successfully reproduced a nonlinear rapid increase at 30° and 210° associated with the turbulent transition. Furthermore, the phase 80° where the wall-shear stress is the largest coincide with the conventional LES. Turbulent mixing reduces the phase lag between the wall-shear stress and the freestream to less than 90° in laminar flow case(Salon et al., 2007).

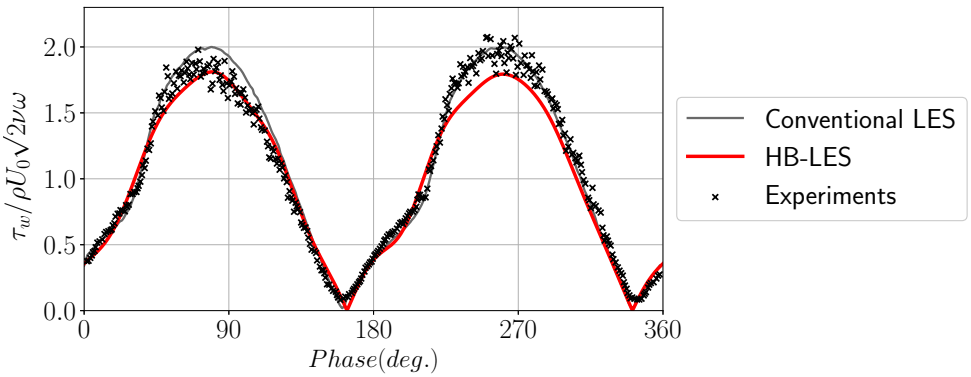

Figure 4 Evolution of Normalized Wall-Shear Stress $\tau_w/\rho U_0\sqrt{2\nu\omega}$ over One Period, legends are the same as in Fig.3.

Fig.5 shows the profiles of normalized turbulence intensities at $30°, 90°, 150°$. Overall, the agreements between HB-LES and conventional LES are satisfactory. The lower turbulent intensity in the outer layer at 30° is probably owing to excessive decay of free-stream turbulence. These results indicate that the HB-LES accurately predict the periodic components as shown in Fig.3 and 4, because the turbulence statistics are obtained with high fidelity in the LES.

The computation time for Stokes boundary layer is reduced to approximately $1/200$ compared to the conventional LES for 15 periods(Salon et al., 2007). The computational cost for the HB-stage is negligibly small compared to that for the LES-stage. As the time integrations in the LES-stages are completely independent at each time-level, they could be run in parallel. The simulation time for each LES-stage is 0.01 period and convergence is achieved after 8 iterations, so the total computation time of HB-LES is comparable to that required to analyze 0.08 period in conventional LES.

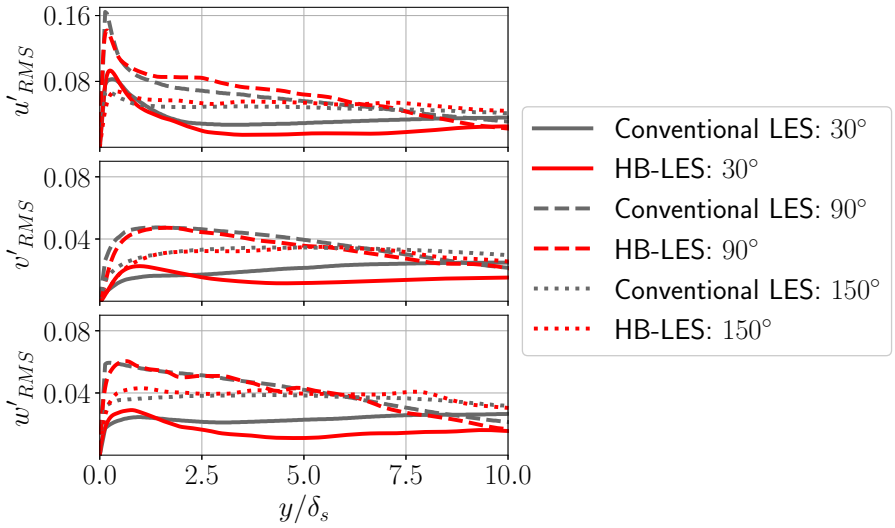

Figure 5 Non-dimensional Turbulent Intencities, red line: HB-LES, black line: conventional LES(C4)(Salon et al., 2007), solid line: 30°, dashed line: 90°, dotted line: 150°.

Pitching NACA0012 Airfoil

As a demonstration of HB-LES, the analysis of dynamic stall on a pitching NACA0012 airfoil (Lee and Gerontakos, 2004; Geng et al., 2018; Wang et al., 2010; Kim and Xie, 2016) is planned in this study. It is known that unsteady turbulence phenomena including transitions, large-scale separation, and relaminarization play important roles in the onset and aerodynamic characteristics of dynamic stalls(Mccroskey, 1981; Visbal and Garmann, 2018; Benton and Visbal, 2019) Although scale-resolving simulation is expected to provide reliable prediction of the dynamic stall, it can be highly time-consuming because of the small nondimentional frequency of $St \simeq 0.01$.

The dynamic stall of a pitching NACA0012 airfoil involves vortex shedding with a frequency shorter than that of pitching but longer than that of turbulent fluctuations. In order to confirm the convergence of the HB-LES for flows involving vortex shedding, the simulation of a NACA0012 airfoil pitching with small amplitude is run as a preliminary study. The pitching movement is given by

$$\alpha(t) = \alpha_0 cos(\omega t) \tag{8}$$

about $x/c = 0.25$ where $\alpha_0 = 1$ deg and the non-dimensional frequency $(c/U_0)/T = 0.1$. The Reynolds number based on the freestream velocity U_0 and the coord length c is 2×10^5. U_0 is coresspoding to the Mach number of $M_0 = 0.15$. The conventional LES with real-time integration is also performed for the comparison with HB-LES.

The C-type mesh with $813 \times 255 \times 41$ grid points is used.A wake length and a domain radius are of $10c$ and span-wise length is $0.05c$. The maximum grid spacing on the airfoil are $\Delta x^+ \sim 60, \Delta y^+{}_{min} \sim 1.0, \Delta z^+ \sim 15$. The flow is periodic for the spanwise directions. Far-field boundary condition at the outer edges and no-slip wall boundary condition on the airfoil are imposed, respectively.

Fig.6 is the spectrum of the lift coefficient C_L of the conventional LES. The peak around 330 Hz is attributed to vortex shedding from the trailing edge. In HB-LES, only the flow oscillation correlated with pitching are treated as periodic components. The cutoff frequency of low-pass filter is sufficiently smaller than the frequency of vortex shuedding, and the simulation time of each LES-stage is $\Delta T = 1/7T$. The number of harmonics $N = 2$ is chosen based on a mode convergence of the conventional HB for pitching airfoils (J.P.Thomas et al., 2009; Cagnone and Nadarajah, 2009).

Fig.7 shows the lift hysteresis. In the results of conventional LES for three periods, the C_L value is approximately 0.1 larger at decreasing case than at increasing case for the same angle of attack. Convergence has not been achieved at stage 10 in the HB-LES. The hysteresis increases once and then decreases again as the stage progresses, which is considered to be a convergence process. The C_L values of $\alpha = \pm 1^\circ$ at stage 10 are close to those of the conventional LES, and hysteresis may be restored with further stages.

CONCLUSIONS

Harmonic balanced large-eddy simulation(HB-LES) is proposed as an acceleration method for the LES of the oscillating flows with the low non-dimensional frequency. HB method for unsteady RANS simulation is originally introduced to LES, utilizing the difference between the period of flow oscillation and the timescale of turbulent fluctuations. Turbulent fluctuations at several time points are resolved by performing multiple short-time integrations. Periodic flow is solved by convergence calculation of the HB method. The convergence calculation and time integrations are alternatively iterated

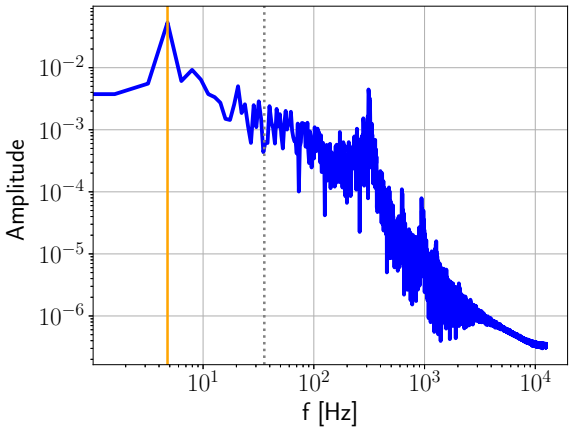

Figure 6 Spectrum of Lift Coefficient, orange line: pitching frequency, dotted gray line: cut-off frequency of HB-LES.

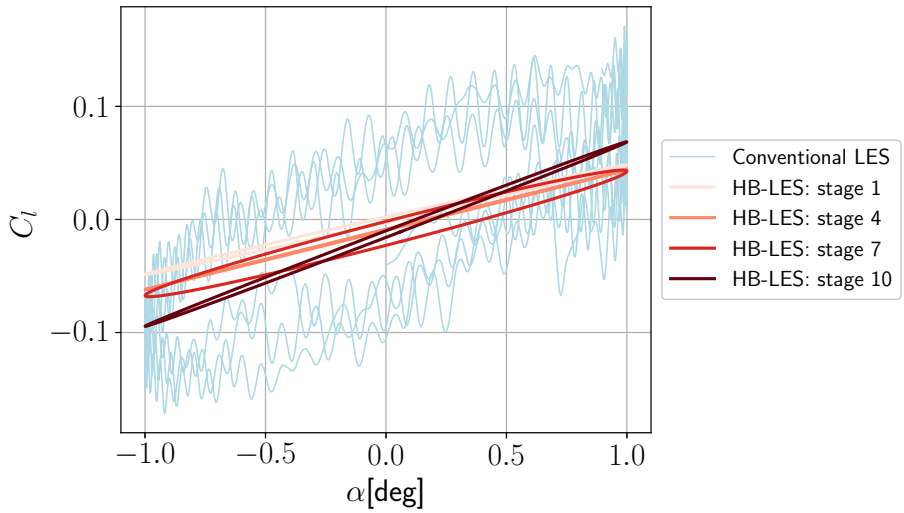

Figure 7 Lift Hysteresis of Pitching NACA0012, lightblue line: conventional LES, red lines: HB-LES.

exchanging their results to compute the nonlinear mutual interaction between turbulent fluctuation and periodic flow.

The HB-LES is applied to the analysis of a Stokes boundary layer at the Reynolds number of 1790. The periodic components and turbulent statistics of the HB-LES show good quantitative agreement with the experimental and conventional LES. The computation time is reduced to approximately $1/200$ of that for the conventional LES.

The analysis of dynamic stall on a pitching NACA0012 airfoil is planned as a demonstration of HB-LES. We are now conducting the computation of the flow around a NACA0012 airfoil pitching with small amplitude as a preliminary study.

NOMENCLATURE

c	=	coord length	T	=	period
e	=	total energy density	ΔT	=	simulation time in LES-stage
f_c	=	cut-off frequency for low-pass filter	U	=	representative velocity
f_p	=	fundamental frequency of periodic component	u, v, w	=	velocities
f_t	=	representative frequency of turbulent fluctuations	x, y, z	=	Cartesian coordinates
L	=	representative lenght or low-pass filter	α	=	coefficient of compact filter
N	=	maximum Fourier index of periodic component	δ_S	=	Stokes boundary layer thickness
p	=	static pressure	ω	=	fundamental angular frequency
$\mathbf{Q}$	=	conservative variables	ρ	=	density
$\mathbf{R}$	=	right-hand side values	τ	=	shear stress
$\mathbf{S}$	=	source term	$\hat{}$	=	periodic components
S_t	=	Strouhal number	$'$	=	turbulent fluctuation components
t	=	time	$^+$	=	normalized quantity by wall unit

ACKNOWLEDGMENTS

This work was supported by JST SPRING, Grant Number JPMJSP2108.

REFERENCES

References

Benton, S. I. and Visbal, M. R. (2019), 'The onset of dynamic stall at a high, transitional reynolds number', *Journal of Fluid Mechanics* **861**, 860–885.

Cagnone, J. and Nadarajah, S. (2009), 'Implicit nonlinear frequency-domain spectral-difference scheme for periodic euler flow', *AIAA Journal* **47**(2), 361–372.

Denton, J. D. (2010), Some Limitations of Turbomachinery CFD, Vol. Volume 7: Turbomachinery, Parts A, B, and C of *Turbo Expo: Power for Land, Sea, and Air*, pp. 735–745.

Fujii, K. and Obayashi, S. (1989), 'High-resolution upwind scheme for vortical-flow simulations', *Journal of Aircraft* **26**(12), 1123–1129.
URL: *https://doi.org/10.2514/3.45890*

Gaitonde, D. V. and Visbal, M. R. (2000), 'Pade-type higher-order boundary filters for the navier-stokes equations', *AIAA journal* **38**, 2103–2112.

Geng, F., Kalkman, I., Suiker, A. and Blocken, B. (2018), 'Sensitivity analysis of airfoil aerodynamics during pitching motion at a reynolds number of 1.35×105', *Journal of Wind Engineering and Industrial Aerodynamics* **183**, 315–332.
URL: *https://www.sciencedirect.com/science/article/pii/S0167610518301806*

Gourdain, N., Sicot, F., Duchaine, F. and Gicquel, L. (2014), 'Large eddy simulation of flows in industrial compressors: a path from 2015 to 2035', *Philosophical Transactions of the Royal Society A: Mathematical, Physical and Engineering Sciences* **372**(2022), 20130323.

Hall, K. C., Ekici, K., Thomas, J. P. and Dowell, E. H. (2013), 'Harmonic balance methods applied to computational fluid dynamics problems', *International Journal of Computational Fluid Dynamics* **27**, 52–67.

Hall, K. C., Thomas, J. P. and Clark, W. S. (2002), 'Computation of unsteady nonlinear flows in cascades using a harmonic balance technique', *AIAA Journal* **40**(5), 879–886.
URL: *https://doi.org/10.2514/2.1754*

He, L. and Yi, J. (2019), 'Two-scale methodology for urans/large eddy simulation solutions of unsteady turbomachinery flows', *Journal of Turbomachinery* **139**(10).

Iwamoto, Y., Teramoto, S. and Okamoto, K. (2022), 'Computationally efficient large-eddy simulation of periodic unsteady flow using harmonic balance method', *Journal of Thermal Science* **31**(1).

Jensen, B. L., Sumer, B. M. and FredsÃ¸e, J. (1989), 'Turbulent oscillatory boundary layers at high reynolds numbers', *Journal of Fluid Mechanics* **206**, 265–297.

J.P.Thomas, C.H.Custer, E.H.Dowell and K.C.Hall (2009), *Unsteady Flow Computation Using a Harmonic Balance Approach Implemented About the OVERFLOW 2 Flow Solver*.
URL: *https://arc.aiaa.org/doi/abs/10.2514/6.2009-4270*

Kim, J. W. and Lee, D. J. (1996), 'Optimized compact finite difference schemes with maximum resolution', *Aiaa Journal - AIAA J* **34**, 887–893.

Kim, J. W. and Lee, J. D. (2011), 'Implementation of boundary conditions for optimized high-order compact schemes', *Journal of Computational Acoustics* **05**.

Kim, Y. and Xie, Z.-T. (2016), 'Modelling the effect of freestream turbulence on dynamic stall of wind turbine blades', *Computers & Fluids* **129**, 53–66.

Kurokawa, M., Teramoto, S. and Okamoto, K. (2020), 'Acoustic wave generation from two-dimensional supersonic inviscid jet impinging on inclined plate', *AIAA Journal* **58**(8), 3436–3445.

Lee, T. and Gerontakos, P. (2004), 'Investigation of flow over an oscillating airfoil', *Journal of Fluid Mechanics* **512**, 313–341.

Mayle, R. E. (1991), The Role of Laminar-Turbulent Transition in Gas Turbine Engines, Vol. Volume 5: Manufacturing Materials and Metallurgy; Ceramics; Structures and Dynamics; Controls, Diagnostics and Instrumentation; Education; IGTI Scholar Award; General of *Turbo Expo: Power for Land, Sea, and Air*. V005T17A001.

Mccroskey, W. J. (1981), The phenomenon of dynamic stall., Technical Report ADA098191, National Aeronautics and Space Administration, Scientific and Technical Information Office ; For sale by the National Technical Information Service.

Salon, S., Armenio, V. and Crise, A. (2007), 'A numerical investigation of the Stokes boundary layer in the turbulent regime', *Journal of Fluid Mechanics* **570**, 253–296.

Slotnik, J., Khodadoust, A., Alonso, J., Darmofal, D., Gropp, W., Lurie, E. and Mavriplis, D. (2014), Cfd vision 2030 study: A path to revolutionary computational aerosciences, Technical Report CR-2014-0218178, National Aeronautics and Space Administration, Scientific and Technical Information Office ; For sale by the National Technical Information Service.

Teramoto, S. (2005), 'Large-eddy simulation of transitional boundary layer with impinging shock wave', *AIAA Journal* **43**(11), 2354–2363.

Teramoto, S., Sanada, H. and Okamoto, K. (2017), 'Dilatation effect in relaminarization of an accelerating supersonic turbulent boundary layer', *AIAA Journal* **55**(4), 1469–1474.

Visbal, M. R. and Garmann, D. J. (2018), 'Analysis of dynamic stall on a pitching airfoil using high-fidelity large-eddy simulations', *AIAA Journal* **56**(1), 46–63.
URL: *https://doi.org/10.2514/1.J056108*

Wang, S., Ingham, D. B., Ma, L., Pourkashanian, M. and Tao, Z. (2010), 'Numerical investigations on dynamic stall of low reynolds number flow around oscillating airfoils', *Computers & Fluids* **39**(9), 1529–1541.
URL: *https://www.sciencedirect.com/science/article/pii/S0045793010001106*

Xiao, H. and Jenny, P. (2012), 'A consistent dual-mesh framework for hybrid les/rans modeling', *Journal of Computational Physics* **231**(4), 1848–1865.
URL: *https://www.sciencedirect.com/science/article/pii/S0021999111006516*